Pergamon

Int. J. Heat Mass Transfer. Vol. 38, No. 18, pp. 3475–3484, 1995

0017-9310/95 $9.50+0.00

0017-9310(95)00037-2

Experimental studies of laminar flow and heat transfer in a one-porous-wall square duct with wall injection

Y. C. CHENG† and G. J. HWANG‡

Department of Power Mechanical Engineering, National Tsing Hua University, Hsinchu 30043, Taiwan, Republic of China

(*Received* 2 *September* 1994 *and in final form* 12 *January* 1995)

Abstract—Experiments were conducted to investigate the effect of fluid injection on laminar flow and heat transfer characteristics in a one-porous-wall square duct. Uniform air flow at $Re_0 = 400$–2000 entered the duct with a cross section of 20×20 mm^2 and a ratio of the active injection length to the hydraulic diameter of 40. Pressurized air was injected through a thick layer of porous material for flow uniformity and a heated porous duct wall at injection rates $Re_w = 5$–20. All of the measured and deduced data, including the axial velocity profiles, the pressure drops, the friction factors, the porous wall temperatures, the outlet fluid temperatures and the Nusselt numbers, were presented and compared with the previous theoretical results. The deduced friction factors and Nusselt numbers from the experimental data were correlated within differences of $\pm 10\%$ and $\pm 15\%$ respectively.

INTRODUCTION

The internal laminar flow in a duct with fluid injection or suction and heat transfer at the porous wall has been investigated extensively for many engineering applications, including the design and analysis of nuclear reactors, combustion chambers, food-drying processes, heat pipes, solar air collectors, fuel cell stacks and purification processes by reverse osmosis. Olson [1] performed a one-dimensional analysis of laminar flow in porous pipes. Later, Berman [2] presented a two-dimensional analysis for fully-porous channels. Some similar studies were contributed by Donoughe [3] for semiporous channels, Yuan and Finkelstein [4] for porous pipes as well as Berman [5] for porous annular tubes. Research into combined laminar flow and heat transfer in porous pipes was introduced by Yuan and Finkelstein [6], and that into porous channels was initiated by Terrill [7]. Since then, many related research works have been carried out, some of the results can be referred to in the brief review of Kays and Perkins [8].

Most of the studies were focused on theoretical analysis; only a few experimental works on the laminar flow are listed in Table 1. Wageman and Guevara [9] studied the laminar flow through a porous pipe with fluid suction, and the flat character of the axial velocity profiles for suction flow was verified. Bundy and Weissberg [10] carried out an experimental work of fully developed flow in a porous pipe with wall injection. The variations of axial pressure gradients and the ratios of centreline to mean velocities were reported. Later, Kohler [11] investigated the laminar flow through a semiporous channel and found the existence of slip conditions on the porous wall for slow flow ($Re_0 < 4$) with weak suction. However, this result had not been reported by other researchers for fast duct flow. Raithby and Knudsen [12] studied the flow in fully porous channels with strong wall suction, and concluded that the flow cannot be fully developed for high suction rates. More measurements were conducted by Quaile and Levy [13] for a suction flow in porous pipes. Unstable reverse flow was observed for $Re_w < -4$, pressure gains were found for $Re_w < -2$, and locations of points of flow separation were also presented. It is seen that nothing for the corresponding heat transfer problem can be found in the literature.

Recently, Hwang *et al.* [14] carried out a theoretical study for laminar developing flow in a one-porous-wall square duct with fluid injection or suction and a constant wall heat flux. According to the results for the injection flow, the peak of the axial velocity profile is shifted away from the porous wall towards the opposite solid wall. The pressure drop and friction factor for the injection flow are increased along the duct compared with those for an impermeable flow. In the heat transfer problem the temperatures of both the heated porous wall and the duct fluid are increased with the wall injection. The Nusselt number is decreased by fluid injection. Moreover, the correlations of friction factors and Nusselt numbers were also deduced [15].

† Current address: Energy and Resources Laboratories, ITRI, Chutung 310, Taiwan.

‡ Author to whom correspondence should be addressed.

NOMENCLATURE

A	cross-sectional area
c_p	specific heat at constant pressure
D	side length of a square duct
D_h	hydraulic diameter, $4A/S$
Ec	Eckert number, $\bar{U}^2/[c_p(\overline{T_w}-T_b)]$
f	friction factor, $2\tau_w/(\rho\bar{U}^2)$
h	heat transfer coefficient, $q/(\overline{T_w}-T_b)$
k	thermal conductivity
L	axial length of a test section
Nu	local Nusselt number, hD/k
P, p	pressure and dimensionless pressure averaged over a cross section, $p = P/(\rho U_0^2)$
Pr	Prandtl number, v/α
q	heat flux on the porous wall
Re_0	inlet Reynolds number, U_0D/v
Re_w	wall Reynolds number, V_wD/v
S	wetted perimeter
T	temperature of fluid
ΔT	temperature difference between the inlet and the outlet of a duct
U, V, W	velocity components in the X, Y and Z directions
u, v, w	dimensionless velocity components in the x, y and z directions, U/U_0, VD/v, WD/v
X, Y, Z	rectangular coordinates
x, y, z	dimensionless rectangular coordinates, $X/(DRe_0)$, Y/D, Z/D.

Greek symbols

η, η^+	normalized axial coordinates for fRe and Nu correlations respectively
θ	dimensionless temperature, $(T-T_0)/(qD/k)$
μ	viscosity
v	kinematic viscosity
ρ	density
τ	shear stress.

Subscripts

b	bulk fluid condition
c	centre point of cross section
f	mainstream
fd	values in the fully developed region
j	injection fluid
m	average value over an axial distance
w	wall condition
0	inlet condition.

Superscripts

−	cross-sectional average at a fixed axial location
+	definition for $x^+ = x/Pr$.

Table 1. Previous studies on laminar and turbulent flow in porous ducts

Investigators	Year	Geometry	D_h (mm)	L/D_h	Initial condition†	Boundary condition‡	Range of Re_0	Range of Re_w
Wageman and Guevara [9]	1960	○	—	—	—	Ⓢ	—	—
Bundy and Weissberg [10]	1970	○	35	85	HF	Ⓘ	0–1000	0–14
Kohler [11]	1972	=	17	10	HD	Ⓢ	0.2–8	0–0.12
Raithby and Knudsen [12]	1974	=	64	4	HD	Ⓢ	300–4800	−10−−20
Quaile and Levy [13]	1975	○	9.4	13	HF	Ⓢ	200–1000	0−−30

†HF = hydrodynamically developing flow, HD = hydrodynamically developed flow.
‡Ⓘ = injection flow, Ⓢ = suction flow.

In the present work, an experimental system was built for measuring the data of axial velocity distributions, pressure variations, wall temperature variations, as well as the bulk mean fluid temperatures at the inlet and outlet of a one-porous-wall square duct with various fluid injection rates. After the pressure variation along the duct axis and the flow rate were measured, the friction factor could be deduced. In addition, the mean Nusselt numbers could be computed from the measured wall temperatures and deduced bulk mean temperatures. A comparison of the present experimental data with the theoretical results [14, 15] is also made.

PHYSICAL MODEL

The flow and heat transfer characteristics in a one-porous-wall square duct with wall injection are more complex than those for solid walls. Consider a steady laminar flow of an incompressible fluid with constant

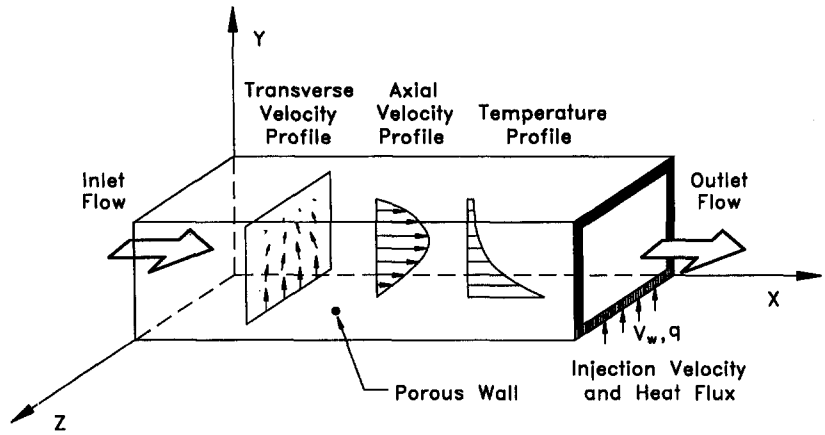

Fig. 1. Physical model and coordinates.

physical properties in a square duct, as shown in Fig. 1. The lower duct wall is porous and subjected to a constant heat flux, while the other three walls are impermeable and adiabatic. The entry velocity and temperature profiles of the axial mainstream are uniform. A fluid flow is injected uniformly into the duct flow through the porous wall. The injected fluid is the same as that of the mainstream and has the same temperature of the heated porous wall.

According to the theoretical results of Hwang *et al.* [14], the duct flow development is caused by both the entrance and injection effects. As pictured in Fig. 1, the axial velocity profile is on a centreline perpendicular to the bottom porous wall. Because of the mass input from the porous wall, the axial velocity is increased and its peak is shifted towards the opposite upper solid wall. Because of a constant mass flux transferred through the porous wall, the larger transverse velocity in the lower area of a cross section is always observed. The overall continuity equation can be obtained by using the mass balance as

$$\bar{u} = \frac{\bar{U}}{U_0} = \frac{Re}{Re_0} = 1 + Re_w x \tag{1}$$

where $Re = \bar{U}D/\nu$ is the local Reynolds number, $Re_0 = U_0 D/\nu$ is the inlet Reynolds number, $Re_w = V_w D/\nu$ is the wall Reynolds number indicating the injection rate and $x = X/(DRe_0)$ is the dimensionless axial distance.

The local peripheral Fanning friction factor is defined as $f = \overline{\tau_w}/(\rho \bar{U}^2/2)$, where $\overline{\tau_w}$ is the peripheral average shear stress over the four walls and $\bar{U}$ is the average axial velocity over the cross section at a specific axial location. The friction factor is large at the duct inlet, and decreases along the axial distance. Obviously, the wall shear stress $\overline{\tau_w}$ is determined by the inlet axial velocity, U_0, the side length, D, the axial location, X, the injection speed, V_w, as well as by the physical properties of the fluid, ρ and μ. Seven dimensional variables and three dimensions, i.e. mass, length and time, are found. Thus, four dimensionless parameters can be derived in the system. The Poiseuille number or the product of the local friction factor and the Reynolds number is a function of x, Re_0 and Re_w. Because of the large Reynolds number, $Re_0 = 400$–2000, in the experiment, the axial viscous force can be neglected. The parameter Re_0 showing the effect of inertial force is already absorbed in the dimensionless axial distance, $x = X/(DRe_0)$ [14]. Therefore, the result is

$$fRe = F(x, Re_w) \tag{2}$$

where Re can be related to x, Re_0 and Re_w as shown in equation (1). According to the coordinate system shown in Fig. 1, the value of Re_w is positive for an injection flow, negative for a suction flow and zero for an impermeable flow.

Considering also the overall force balance for a unit axial length in the X-direction as

$$\rho \frac{d\overline{U^2}}{dX} + \frac{dP}{dX} = -\frac{4}{D}\overline{\tau_w} \tag{3}$$

where $\rho\overline{U^2}$ is the average inertia force, $\bar{P}$ is the average pressure and $\overline{\tau_w}$ is the average shear stress over the four duct wall. By using the dimensionless variables $p = (P - P_0)/\rho U_0^2$ and $\overline{\tau_w^*} = \overline{\tau_w}/(\mu U_0/D)$, the above equation can be rewritten as

$$fRe = \frac{1}{2\bar{u}}\left[\left(-\frac{dp}{dx}\right) - \frac{d\overline{u^2}}{dx}\right]. \tag{4}$$

The temperature of the mainstream fluid increases along the flow direction because of the wall heating effect and the injected thermal energy. As depicted in Fig. 1, the temperature in the lower area is always higher due to the constant heat flux transferred through the porous wall. Moreover, thermal energy addition by injected fluid also increases the fluid temperature in the duct. Obviously, the heat transfer rate is also determined by four additional dimensional variables, i.e. the bulk temperature difference $\overline{T_w} - T_0$, the heating rate, q, and the physical properties of the

fluid, c_p and k. One more dimension, i.e. temperature, is included. Therefore three more parameters Nu, Pr and Ec can be derived. Neglecting the viscous dissipation, i.e. $Ec = 0$, and using the dimensionless axial distance, $x^+ = X/(Pr\,D\,Re_0)$, the Nusselt number can be written as

$$Nu = F(x^+, Pr, Re_w). \tag{5}$$

It is noted that $Pr = 0.72$ for air is used in the present study. At the duct inlet, the Nusselt number is theoretically infinite due to the sudden application of heat flux. The Nusselt number decreases along the axial distance until it finally attains a constant value [14, 15].

A local heat transfer coefficient, h, which relates to the supply of heat flux from the heated porous wall, may be defined as $h = q/(\overline{T_w} - T_b)$. Therefore, the local Nusselt number can be also expressed as

$$Nu = \frac{hD}{k} = \frac{qD}{k(\overline{T_w} - T_b)} = \frac{1}{\overline{\theta_w} = \theta_b} \tag{6}$$

where $\overline{\theta_w} = \overline{T_w}/(qD/k)$ and $\theta_b = T_b/(qD/k)$ are the average dimensionless wall temperature and the bulk mean fluid temperature respectively. In addition, the mean Nusselt number is taken by using the inverse of the mean value of bulk temperature difference as

$$Nu_m = \frac{1}{(\overline{\theta_w} - \theta_b)_m}. \tag{7}$$

EXPERIMENTAL SYSTEM

As pictured schematically in Fig. 2, an open loop fluid flow facility was used for the experiment. This system consisted of four major parts including an air supply system, a settling chamber, an injection unit and a test section. A 2 hp compressor with air pressure up to $7 \times 10^5\ N\,m^{-2}$ was used for the air supply. Before entering the pressure regulators, two filters and a refrigeration dehydrator were employed for removing oil, water and particulate material greater than 3 μm diameter. One regulator was for controlling the rate of inlet mainstream, and another was for adjusting flow rate of injected flow. Two rotameters used in this system were carefully calibrated, using the bubble method with an accuracy of 2% in the range of 0–$36\ l\,min^{-1}$.

The velocity distribution of supply air was firstly homogenized, using a porous nozzle, and then the air was expanded in a divergent square channel of the settling chamber. This chamber consists of four segments, with a layer of stainless steel mesh, a multilayer cotton cloth, a honey-comb and another stainless steel mesh to depress the turbulent intensity. Finally, the flow was contracted by a 10 : 1 convergent square channel to attain a uniform axial velocity profile.

The injection unit located underneath the test duct was to create a uniform injection velocity through the bottom porous wall along the square duct. As can be seen in Fig. 3, this injection unit was made of four layers of Bakelite plates with the dimensions $870 \times 80 \times 50$ mm. The injected flow was first distributed by a closed-end distribution tube with a series of downward pin holes, having a total open area equal to the cross-section area of the inlet tube. Then, the air flow passed two thick layers of ceramic fibre, a heating layer and a graphite plate with 1 mm thickness for uniform flow distribution. In this unit, most of the flow resistance was produced by the graphite plate with a low permeability. A preliminary test showed that the range of pressure drops across this graphite plate for injection Reynolds numbers of Re_w = 5–20

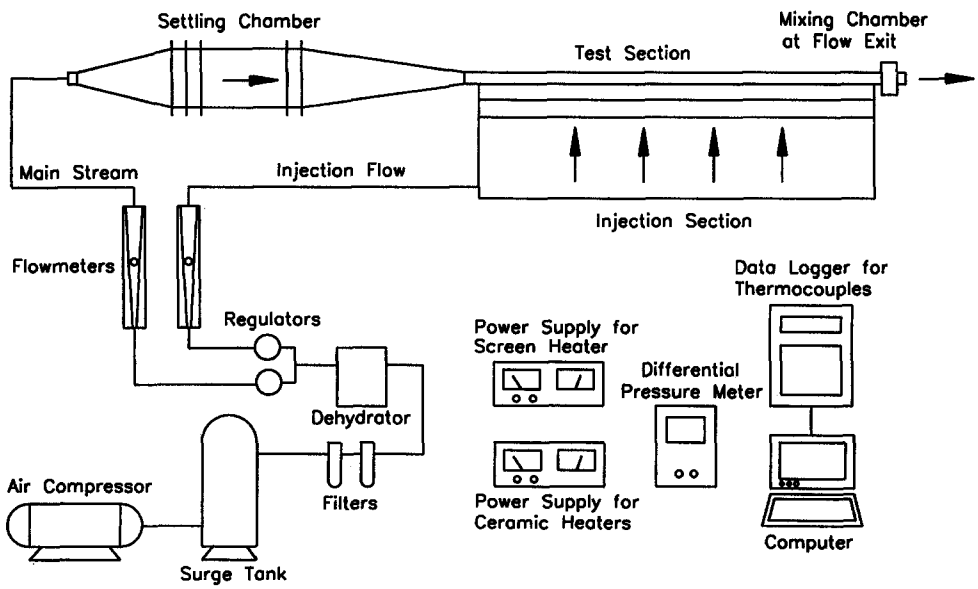

Fig. 2. Schematic flow diagram of experimental set-up.

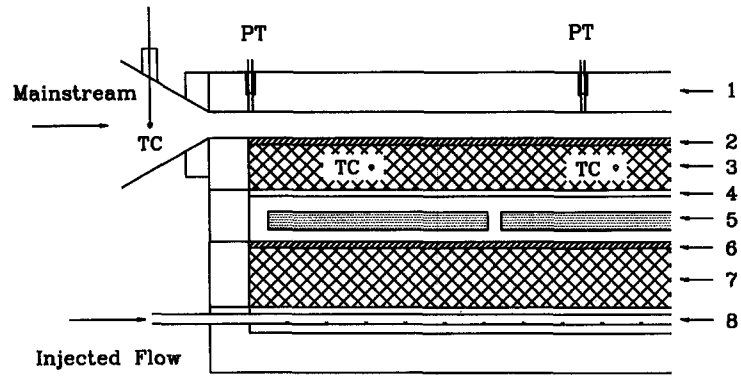

PT=Pressure Tag TC=Thermocouple

1 Acrylic Plate
2 Screen Heater
3 Ceramic Fiber
4 Cotton Fabric
5 Ceramic Heater
6 Graphite Plate
7 Ceramic Fiber
8 Distribution Tube

Fig. 3. Details of test section and injection unit.

is 0.06–0.24 bar, which was large enough compared with the total pressure drop of 0.002 bar for $Re_0 = 2000$ in the mainstream of the duct. It may be concluded that the injected velocity along the duct wall could maintain its uniformity. However, the fragile nature of the graphite plate was a serious problem, thus a supporting perforated frame had to be installed as well. In the heating layer, four ceramic heaters were installed for raising the temperature of the injection flow. These heaters were connected to four independent DC power supplies for easy control of the injection temperature along the test duct. The major considerations in using the ceramic heaters were their high heating efficiency and compact configuration.

As also shown in Fig. 3, the lower wall of the square-duct test section was composed of a sheet of stainless steel screen (Mesh 325) with effective surface area about 20×800 mm and three thin layers of ceramic fabric which are not shown explicitly in this figure. The metal screen was connected to a DC power supply to form a heating porous wall. Under the screen, pairs of thermocouples were welded along the mainstream direction for temperature measurement. In addition, the upper wall was a piece of transparent acrylic plate for flow observation, and the other two side walls were also assemblies of Bakelite plates. The duct had an effective dimension of $20 \times 20 \times 800$ mm with a ratio of the active axial length to the hydraulic diameter of 40.

Five pressure taps at 0, 200, 400, 600 and 800 mm locations from the inlet edge were inserted at the upper plate along the channel. The static pressures were read by a micro-manometer with an accuracy of 2%. The velocity profile at the exit of the test section was measured by a Pitot tube, the readings were also taken by the same micro-manometer. Temperatures were measured by pairs of T-type thermocouples. The inlet fluid temperatures were measured at the exits of rotameters for the flow-rate calculation. Two pairs of thermocouples were installed at the inlet and outlet of the channel, 13 pairs of thermocouples were used for detecting the porous wall temperatures, and the other four pairs of thermocouples were inserted into the injection unit for monitoring the injection air temperature along the duct. Each pair of thermocouples was connected to a data logger with a multi-channel chart recorder. All of the readings from the data logger and micro-manometer can be recorded by a personal computer for further data processing. Table 2 depicts the ranges of the experimental variables and the corresponding parameters.

DATA REDUCTION

Since experiments were performed with a moderate temperature difference and pressure difference across the test section, fluid property variations did not play a major role in the data reduction. Typically, the inlet bulk temperature of the main flow was about 25–

Table 2. Experimental variables for the present study

Variable	Range of measurement
Re_0	400, 450, 500, 600, 800, 1000, 1200, 1500, 2000
Re_w	0, 5, 10, 20
ΔP_f (mm H_2O)	0.04–0.80
ΔP_j (mm H_2O)	50–200
X/D_h (Pressure tap)	0, 10, 20, 30, 40
ΔT [°C]	2.4–6.6
T_{wm} [°C]	40.2–51.6
Pr	0.72
X [cm] (Thermocouples)	1, 5, 10, 15, 20, 25, 30, 35, 40, 50, 60, 70, 79

30 °C, and the fluid temperature difference between the inlet and outlet of the test section was lower than 10 °C, and the air temperature in the injection flow was not higher than 50 °C. The physical properties were evaluated at the mean value of the bulk flow and wall temperatures at each specific location of the duct. The value of the Prandtl number used in the evaluation of the Nusselt number was 0.72.

At a certain axial location, the local friction factor fRe was evaluated from equation (4), using the average axial velocity $\bar{u}$, the pressure gradient $(-\mathrm{d}p/\mathrm{d}x)$ and the axial inertia variation $(\mathrm{d}\overline{u^2}/\mathrm{d}x)$. The axial velocity was computed from equation (1), and the axial inertia variation was directly taken from the numerical results of Hwang *et al.* [15]. The measured pressure data were correlated into the simple form of second-order polynomial equations in three different segments along the duct length, i.e. $0.005 < x \leqslant 0.01$, $0.01 < x \leqslant 0.03$ and $0.03 < x \leqslant 0.1$. The discrepancy between the experimental data and these equations was dependent on the axial distance and the wall Reynolds number. In the inlet region, the error might be as large as $\pm 15\%$. However, the errors of most data were found within $\pm 6\%$. These polynomials were used for the evaluation of the pressure gradient [16].

The determination of the value of the local Nusselt number involved the local heat flux, q, and the local wall and bulk temperatures, T_w and T_b. Since it was difficult to measure the bulk mean fluid temperature at each specific axial location, the Nusselt number could not be computed directly from the experimental data. The method of deduction of the bulk mean fluid temperatures from the measured data will now be discussed. The bulk temperature at any axial position, X, can be evaluated from an energy balance on a square control volume between X and $x+\mathrm{d}X$. Note that the following equation applies at any axial position

$$qD\,\mathrm{d}X = [\rho c_p(\bar{U}+\mathrm{d}\bar{U})(T_b+\mathrm{d}T_b) - \rho c_p \bar{U} T_b]D^2 - \rho c_p V_w \overline{T_w} D\,\mathrm{d}X. \quad (8)$$

Combining this with equation (1), the equation of bulk temperature can be obtained:

$$\frac{\partial \theta_b}{\partial x^+} + \frac{Pr\,Re_w}{1+Pr\,Re_w x^+}\theta_b = \frac{1+Pr\,Re_w\overline{\theta_w}}{1+Pr\,Re_w x^+}. \quad (9)$$

The solution of equation (9), subjected to its initial condition $\theta_b = 0$ at $x^+ = 0$, is

$$\theta_b = \frac{1}{1+Pr\,Re_w x^+}\int_0^{x^+}(1+Pr\,Re_w\overline{\theta_w})\,\mathrm{d}x^+. \quad (10)$$

Therefore, the bulk temperature at each axial location could be computed from the inlet temperature of the mainstream and the measured temperatures of the heated porous wall. According to the calculation results of the present study, the difference between the calculated and measured temperatures at the outlet of the duct was usually lower than 5%.

Invoking the method suggested by Kline and MaClintock [17], an uncertainty analysis was performed to estimate the uncertainties in the reported results. The relative uncertainty in the axial velocities measured by the rotameters was estimated to be within $\pm 2.8\%$. However, the relative uncertainties of the axial velocities measured by the Pitot tube might be as low as $\pm 1.3\%$ in the centre point of a cross-section and as high as $\pm 9.3\%$ at the position near the duct boundaries. The local friction factor used in this study was deduced from equation (4), and its error attributed mainly to the first term on the right-hand side. Based on the estimated uncertainties of the static pressure measurements of $\pm 2.7\%$ at high values and $\pm 13.1\%$ at low values, the uncertainties in fRe were estimated to be $\pm 3.4\%$ and $\pm 13.2\%$ respectively.

All of the thermocouples used in the measurements and the corresponding readings of the data logger were carefully calibrated with an accuracy of ± 0.2 °C. On the other hand, the accuracies of the multimeter, which is used for measuring the heating rate, were $1.5\% + 2$ digital for current measurement and $0.3\% + 1$ digital for voltage measurements. Therefore, the largest estimated uncertainty of the mean Nusselt number was not higher than 10% in all measured data.

RESULTS AND DISCUSSION

The experimental data are presented and discussed in the following paragraphs to explore the characteristics of laminar duct flow and heat transfer with wall injection. The previous numerical results [14, 15] are plotted by the line drawings for comparison in Figs. 4–11, and the measured and the deduced data are labelled with remarks.

Reliability of experimental data

Before the verification of the test results with the wall injection, experiments were conducted for zero injection, $Re_w = 0$, to determine the axial centreline velocities, the axial velocity profiles, the pressure

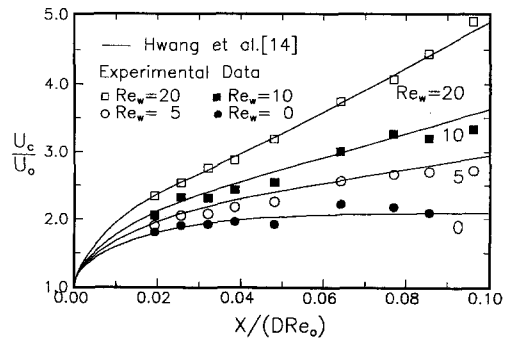

Fig. 4. Centreline velocities along the axial length for various wall Reynolds numbers.

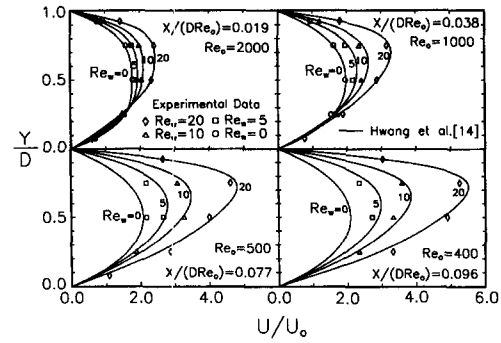

Fig. 5. Axial velocity profiles at specific locations for various wall Reynolds numbers.

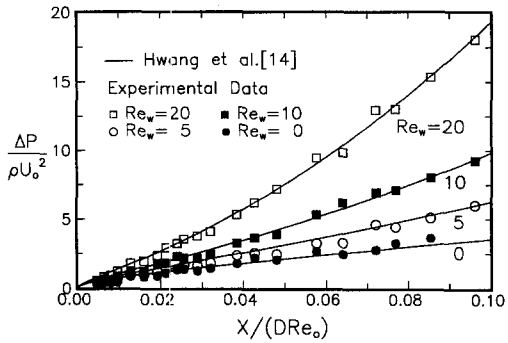

Fig. 6. Pressure drops along the axial length for various wall Reynolds numbers.

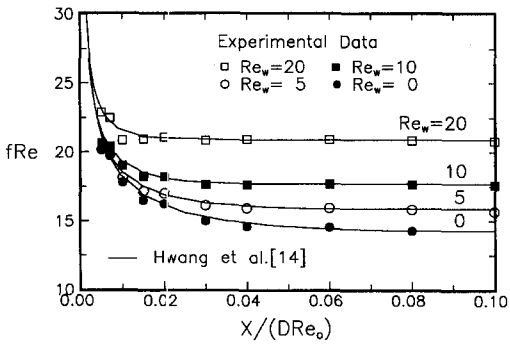

Fig. 7. Friction factors along the axial length for various wall Reynolds numbers.

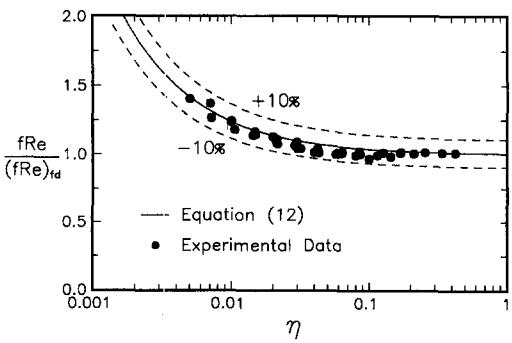

Fig. 8. Comparison of experimental data with previous correlation results of friction factors.

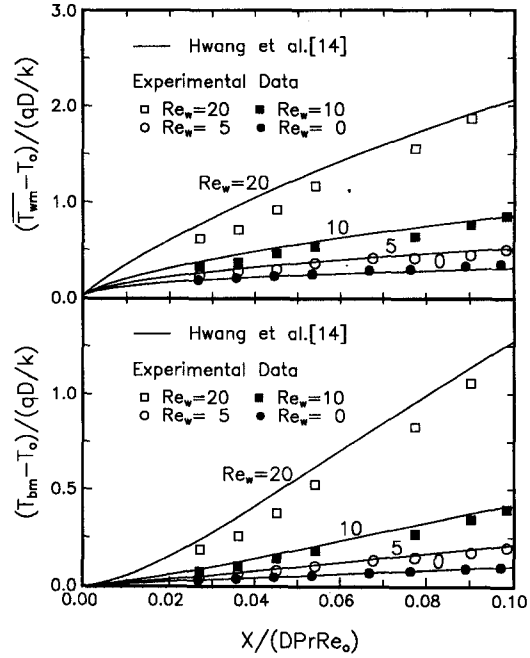

Fig. 9. Porous wall and mixed mean temperatures along the axial length for various wall Reynolds numbers.

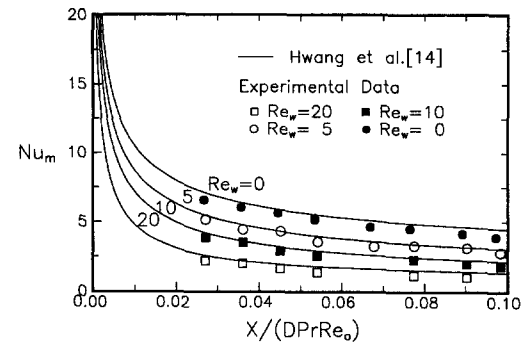

Fig. 10. Nusselt numbers along the axial length for various wall Reynolds numbers.

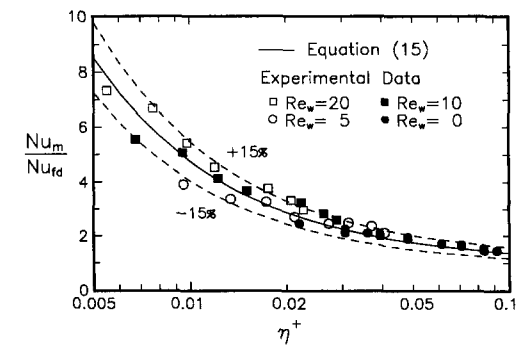

Fig. 11. Comparison of experimental data with new correlation results of Nusselt numbers.

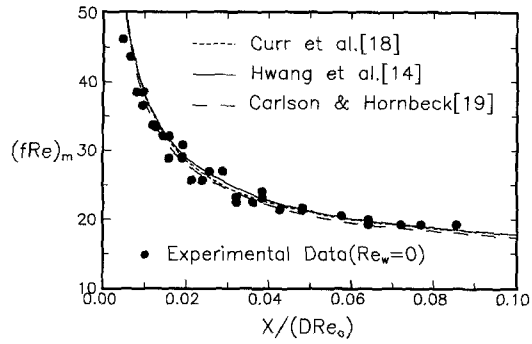

Fig. 12. Comparison of measured friction factors with existing data for duct flow without wall injection.

drops and the local friction factors and heat transfer along the duct for the range of Re_0 from 400 to 2000.

Lacking the corresponding experimental data of friction factors in the developing laminar flow, the theoretical results of Curr *et al.* [18] as well as Carlson and Hornbeck [19] in a square duct are shown in Fig. 12. The average friction factor, f_m, over a specific flow length is defined as

$$f_m = \frac{D(-\Delta P)}{2\rho \bar{U}^2 X} \tag{11}$$

or expressed by $(fRe)_m = -\Delta\rho/(2x) = -\Delta P D^2/(2\mu X U_0)$ in a dimensionless form. The value of $(fRe)_m$ can be calculated directly from the measured inlet average axial velocity and pressure drop at each specific axial location. For comparing with the existing results, the experimental data of impermeable flow are plotted. It is seen in Fig. 12 that most of the experimental data are within $\pm 10\%$ of the existing results. The heat transfer results for zero injection were also measured for various inlet axial velocities and will be discussed later.

Axial velocity distribution and pressure variation

As shown in Fig. 4, experimental results of the ratio of the centreline to the inlet velocity along the duct length for different injection rates are compared with the previous numerical values. The centreline velocity, U_0, was measured on the exit plane of the test section by varying the main flow Reynolds number, Re_0. It is seen that the experimental data are consistent with the theoretical results. As a result of the mass addition and acumulation, the value U_c/U_0 increases with the increase in the value of $X/(D\,Re_0)$ and also the value of Re_w.

Figure 5 shows the dimensionless axial velocity distributions on the exit plane with four injection rates and four dimensionless distances. The measured axial velocity data were taken from five vertical positions, 1.5, 5, 10, 15 and 18.5 mm along the centreline, which is perpendicular to the porous wall, on the duct exit plane. It is seen that the fluid injection increases the axial velocity components of the duct flow and shifts its peak value towards the opposite solid wall. Alhough this movement is not significant near the inlet, the trend is more pronounced as the axial distance increases. This shift is larger for a stronger injection rate because of more fluid injection.

In Fig. 6, a comparison between the measured and theoretical pressure drops along the dimensionless axial length is made for various wall Reynolds numbers. The experimental data fit well the theoretical curve. For the impermeable flow, $Re_w = 0$, the axial pressure continuously decreases in the developing region, and a fixed negative value of the pressure gradient is obtained when the flow is fully developed. For the injection flow, the axial pressure gradient decreases faster than that for the impermeable flow, and this trend becomes more pronounced for larger Re_w. The additional pressure drop is required for overcoming the flow resistance of both viscous and inertial forces, which are increased by the mass addition from the bottom porous wall along the duct.

Friction factor

As shown in equation (4), the local friction factors can be deduced from the measured static pressures. Figure 7 shows the variations of these deduced friction factors along the duct for $Re_w = 0$, 5, 10 and 20. Again, the agreement between the experimental values and the theoretical ones is good. Note that the friction factor is always decreased with an increase in the axial position and is increased with an increase in the injection rate. As shown in Fig. 5, this result can be explained by the steeper axial velocity gradient near the walls for the stronger injection rate. However, a physical interpretation of the full meaning of this phenomenon is needed to understand it further. According to equation (4), the friction factor is affected by both the axial pressure gradient $(-\mathrm{d}p/\mathrm{d}x)$ and the inertial force $(\mathrm{d}\bar{u}^2/\mathrm{d}x)$. As reported previously, the axial inertia variation is gradually decreased along the duct for all of the impermeable flow and injection flows. Hence, the increment of friction factor for $X/(D\,Re_0) \geqslant 0.04$ is mainly produced by the larger pressure gradient.

According to the results of Hwang *et al.* [15], the local friction factors along the axial direction can be correlated as

$$\frac{f\,Re}{(f\,Re)_{fd}} = 1 + 0.00599\eta^{-0.8} \tag{12}$$

where $(fRe)_{fd}$ is the fully developed friction fctor and η is a normalized axial coordinate. The value of $(f\,Re)_{fd}$ is expressed as

$$(fRe)_{fd} = 14.4 + 0.31 Re_w \tag{13}$$

and η is defined as

$$\eta = \frac{x}{(1 - 0.0559 Re_w + 0.00108 Re_w^2)^{1.25}}. \tag{14}$$

The deduced experimental data are presented in Fig. 8 for comparison. The data are within $\pm 10\%$ of the

theoretical correlation for the entire regions of η and Re_w under study.

Temperature variation

For practical applications and theoretical analysis, the average wall temperature, $\overline{\theta_{wm}}$, and the bulk mean temperature of fluid, θ_{bm}, along the duct are of interest. For obtaining these data, experiments were conducted over a range of inlet Reynolds numbers (Re_0 = 550, 600, 700, 800, 1000 1200, 1500 and 2000) with various wall Reynolds number (Re_w = 0, 5, 10 and 20). $\overline{\theta_{wm}}$ and θ_{bm} were evaluated by numerical integration over a certain duct length, where θ_b was computed using equation (10). It can be seen in Fig. 9 that the wall injection increases both the average porous wall temperature and the bulk mean temperature. When a fluid at the same temperature as the heated porous wall is injected into the mainstream, the temperature of fluid in the duct will be increased. Therefore, the temperature of the heated porous wall will also increase in order to maintain the operating condition of constant heat flux.

All experimental data of the average wall temperatures and the bulk mean temperatures are compared with the previous theoretical results in Fig. 9. For all the wall Reynolds numbers, experimental data are slightly lower than those theoretical values of $\overline{\theta_{wm}}$ and θ_{bm} along the dimensionless axial distance except for $Re_w = 0$. The discrepancies of these temperatures are enlarged by the rising injection rate. When an injection flow is introduced into the test section, as shown in Fig. 2, the temperature of the porous wall will rise immediately. It is difficult to maintain the injected fluid at the same temperature as the heated porous wall. To avoid this troublesome problem, the injection temperature was kept 1–2 °C lower than the wall temperature in the experiments. Therefore, the measured wall temperature and the mainstream outlet temperature were all lower than those of the theoretical results.

Heat transfer

In Fig. 10, the variations of Nusselt numbers along the duct for Re_w = 5, 10 and 20 are described. As can be seen in the figure, the experimental data of Nu_m for $Re_w = 0$ agree with the previous theoretical results. Note that the experimental data in the figure are slightly lower than the theoretical values; however, the differences are all within 5%, which is within the uncertainty of 10%, as mentioned previously. It can also be seen that the wall heat transfer is reduced by fluid injection. In the calculation of the Nusselt number, most of the temperature discrepancies for higher Re_w, as shown in Fig. 9, have been cancelled by each other. The agreement between the experimental values and the theoretical ones is fairly good, as shown in Fig. 10. However, most of the measured data are lower than the corresponding theoretical values.

In the present study, the experimental data of Nusselt numbers can be correlated as [20]

$$\frac{Nu_m}{Nu_{fd}} = 1 + \frac{0.0375}{\eta^+} \tag{15}$$

where Nu_{fd} is the fully developed value of the local Nusselt number and η^+ is a normalized axial coordinate. From the results of Cheng [20], the value of Nu_{fd} is expressed as

$$Nu_{fd} = 2.71 - 0.367Re_w + 0.0212Re_w^2 - 0.000443Re_w^3 \tag{16}$$

and η^+ is defined as

$$\eta^+ = \frac{(x^+)^2}{A(x^+) - 0.129B(x^+)^{0.5} + 0.0058C} \tag{17}$$

where the coefficients in the denominator are

$$A = 1 + 0.282Re_w - 0.00631Re_w^2$$

$$B = 1 + 0.384Re_w - 0.00109Re_w^2$$

$$C = 1 + 0.421Re_w - 0.00139Re_w^2. \tag{18}$$

The results of equation (15) are plotted in Fig. 11. The value of Nu_m/Nu_{fd} is decreased with the increase in η^+ and a limiting value of $Nu_m/Nu_{fd} = 1$ for large η^+ is observed. The deduced experimental data are also presented in the figure for comparison. More than 90% of experimental data are within $\pm 15\%$ of the correlated curve for the entire regions of η^+ and Re_w under study.

CONCLUSIONS

In considering the above results and discussion for laminar flow and heat transfer characteristics in a one-porous-wall square duct subjected to a uniform wall injection and a constant heat flux, the following statements can be made.

1. It has been verified experimentally that the friction factor is larger and the Nusselt number is smaller for a larger injection rate.
2. The measured and the deduced data, including the axial velocities, the pressure drops and the friction factors match the predictions of the previous theoretical results.
3. The measured porous wall temperatures, mainstream outlet temperatures and Nusselt numbers can also fit the theoretical results. However, small discrepancies between the experimental and theoretical values are a result of the limitations of the experimental method.
4. The deduced friction factors from the experimental data are within $\pm 10\%$ of the correlation equation. In addition, more than 90% of the deduced Nusselt numbers are within $\pm 15\%$ of the correlated equation for the entire regions of η^+ and Re_w under study.

Acknowledgments—This study is supported by the Energy Commission of the Ministry of Economic Affairs of Taiwan

through Fuel Cell Project no. 833BK1100. The authors also acknowledge the assistance of the Energy and Resources Laboratories, ITRI for the use of their computer.

REFERENCES

1. F. C. W. Olson, Flow through a pipe with a porous wall, *J. Appl. Mech.* **16,** 53–54 (1949).
2. A. S. Berman, Laminar flow in channels with porous walls, *J. Appl. Phys.* **27,** 1232–1235 (1953).
3. P. L. Donoughe, Analysis of laminar incompressible flow in semiporous channels, Tech. Note 3759, NACA (1956).
4. S. W. Yuan and A. B. Finkelstein, Laminar pipe flow with injection and suction through a porous wall, *Trans. ASME* **78,** 719–724 (1956).
5. A. S. Berman, Laminar flow in an annulus with porous walls, *J. Appl. Phys.* **29,** 71–75 (1958).
6. S. W. Yuan and A B. Finkelstein, Heat transfer in laminar pipe flow with uniform coolant injection, *Jet Propulsion* **28,** 178–181 (1958).
7. R. M. Terrill, Heat transfer in laminar flow between parallel porous plates, *Int. J. Heat Mass Transfer* **8,** 1491–1497 (1965).
8. W. M. Kays and H. C. Perkins, Forced convection, internal flow in ducts. In *Handbook of Heat Transfer Fundamentals* (2nd Edn) (Edited by W. M. Rohsenow, J. P. Hartnett and E. N. Gario), Chap. 7. McGraw-Hill, New York (1985).
9. W. E. Wageman and F. A. Guevara, Fluid flow through a porous channel, *Phys. Fluids* **3,** 878–881 (1960).
10. R. D. Bundy and H. L. Weissberg, Experimental study of fully developed laminar flow in a porous pipe with wall injection, *Phys. Fluids* **13,** 2613–2615 (1970).
11. J. T. Kohler, An investigation of laminar flow through a porous-walled channel, Ph.D. Thesis, University of Massachusetts, Amherst, MA (1973).
12. G. D. Raithby and D. C. Knudsen, Hydrodynamic development in a duct with suction and blowing, *J. Appl. Mech.* **41,** 896–902 (1974).
13. J. P. Quaile and E. K. Levy, Laminar flow in a porous tube with suction, *J. Heat Transfer* **97,** 66–71 (1975).
14. G. J. Hwang, Y. C. Cheng and M. L. Ng, Friction factors and heat transfer in a square duct with one-walled injection and suction, *Int. J. Heat Mass Transfer* **36,** 2429–2440 (1993).
15. G. J. Hwang, Y. C. Cheng and M. L. Ng, Friction factors and heat transfer correlations for gaseous reactant flow in fuel cell power modules, *Proceedings of 6th International Symposium on Transport Phenomena in Thermal Engineering*, Vol. 1, pp. 685–690 (1993).
16. R. M. Olson and E. R. G. Eckert, Experimental studies of turbulent flow in a porous circular tube with uniform fluid injection through the tube wall, *J. Appl. Mech.* **33,** 7–17 (1966).
17 S. J. Kline and F. A. MaClintock, Describing uncertainties in single sample experiments, *Mech. Engng* January, 3–8 (1953).
18. R. M. Curr, D. Sharma and D. G. Tatchell, Numerical prediction of some three-dimensional boundary layers in ducts, *Comput. Meth. Appl. Mech. Engng* **1,** 143–158 (1972).
19. G. A. Carlson and R. W. Hornbeck, A numerical solution for laminar entry flow in a square duct, *ASME J. Appl. Mech.* **40,** 25–30 (1973).
20. Y. C. Cheng, Theoretical and experimental study on laminar flow and heat transfer in one-porous-wall ducts, Ph.D. Thesis, National Tsing Hua University, Hsinchu, Taiwan (1994).